

Flexural behavior of precast concrete wall – steel shoe composite assemblies with dry connection

Xiangguo Wu^{1a}, Xinlei Xia^{1b}, Thomas H.-K. Kang^{2c}, Jingcheng Han^{1d} and Chang-Soo Kim^{*3}

¹ Key Lab of Structures Dynamic Behavior and Control of the Ministry of Education,

Key Lab of Smart Prevention and Mitigation of Civil Engineering Disasters of the Ministry of Industry and Information Technology,
Harbin Institute of Technology, 92 West Dazhi Street, Nan Gang District, Harbin, Heilongjiang 150090, China

² Department of Architecture and Architectural Engineering at Seoul National University, 1 Gwanak-ro, Gwanak-gu, Seoul 08826, Korea

³ School of Architecture, Seoul National University of Science and Technology, 232 Gongreung-ro, Nowon-gu, Seoul 01811, Korea

(Received May 5, 2018, Revised October 16, 2018, Accepted October 24, 2018)

Abstract. This study aimed to investigate the flexural behavior of precast concrete (PC) wall – steel shoe composite assemblies with various dry connection details at mid-span. Flexural tests were performed for five scenarios. Test parameters included the width of test specimens, arrangement of steel shoe connectors, and use of structural adhesive or waterproof tape at the mid-span joint. The test results showed that the PC wall – steel shoe composite assemblies joined at mid-span showed flexural damage patterns combined with rotational deformation, and the structural performance was satisfactory regardless of the arrangement of steel shoe connectors. Considering the two deformation components (flexural deformation by bending and rotational deformation due to joint opening), a theoretical model was proposed to analyze flexural strength and joint opening, and the simple model gave good predictions with acceptable accuracy.

Keywords: precast concrete wall; steel shoe; composite assemblies; mid-span joint; dry connection; flexural strength; joint opening

1. Introduction

Use of precast concrete (PC) wall assemblies has benefits in terms of construction speed and quality control, and its application in underground construction in urban areas has been increasing (Kang *et al.* 2014, Lee *et al.* 2016). Generally, PC elements are prefabricated at factories, transported to construction sites, lifted in position, and then assembled to join other elements. Because each PC element is limited in its size due to transportation and lifting limitations, joints are inevitable and their performance is of main concern. PC joints can be categorized into wet-joints and dry-joints, and various joint details have been developed and applied in the field (CAE 1999, Elliott 2002, Englekirk 2003, PCI 2004, fib 2008, Cheng 2008, Ousalem *et al.* 2009, JRC 2012, Lim and Hong 2014, Han *et al.* 2016, Vaghei *et al.* 2016). For large components, a member is divided into PC segments and assembled on site, employing prestressing (Aparicio *et al.* 2002, Saibabu *et al.* 2013, Jiang *et al.* 2016a, b).

In underground structures such as culverts, joints may exist for extension of the substructures or connection to a

superstructure, as well as for transportation and lifting. Fig. 1 shows an example of joints between underground PC wall assemblies. The underground side walls are subjected to lateral forces due to earth and water pressures. In many cases, the underground PC wall segments are assembled using connectors (e.g., steel shoes), and these connectors are placed in consideration of structural performance and construction. Thus, various arrangements of connectors need to be investigated to analyze the flexural behavior of PC wall – steel shoe composite assemblies.

In this study, the flexural behavior of PC wall – steel shoe composite assemblies with various dry connection details at mid-span was investigated. For strength and serviceability design, flexural strength and joint spacing were experimentally and theoretically investigated.

2. Test plan

2.1 Test specimens

To investigate the structural behavior of PC wall – steel shoe composite assemblies, flexural tests were performed for five scenarios. For each scenario, a pair of two symmetric PC wall segments were joined at mid-span through steel shoe connectors. Test parameters included the width of test specimens, arrangement of steel shoe connectors, and use of structural adhesive or waterproof tape at the mid-span joint. Table 1 summarizes the test parameters, and Fig. 2 shows the configuration and dimensions.

*Corresponding author, Ph.D., Associate Professor,
E-mail: changsookim@seoultech.ac.kr

^a Ph.D., Professor

^b Master Student

^c Ph.D., Professor

^d Master Student

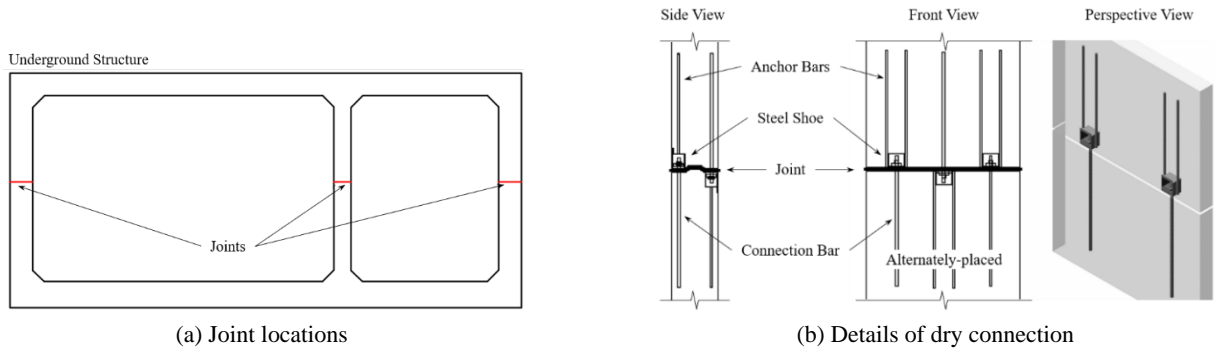


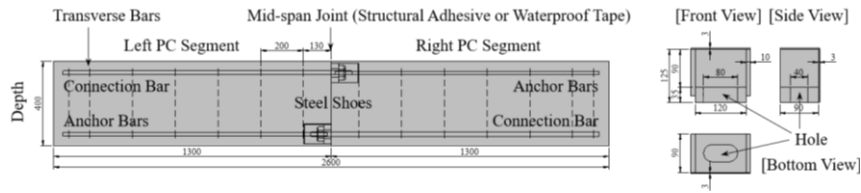
Fig. 1 Example of joints between underground PC wall assemblies

Table 1 Test parameters

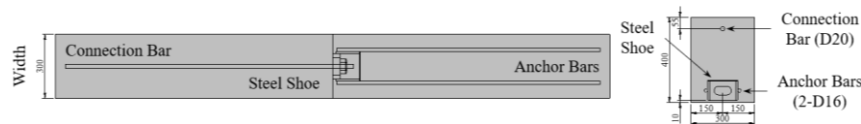
Specimen ¹⁾	Width, b	Arrangement of connectors ²⁾	Structural adhesive	Waterproof tape
S1	300 mm	1 Pair	Applied	No
S2	300 mm	1 Pair	No	Applied
S3	500 mm	2 Pairs (Antisymmetric)	Applied	No
S4	600 mm	2 Pairs (Bisymmetric)	Applied	No
S5	700 mm	3 Pairs	Applied	No

¹⁾ Clear length $L = 2400$ mm, depth $d = 400$ mm, and transverse bars = 8 mm-diameter bars at a spacing of 200 mm

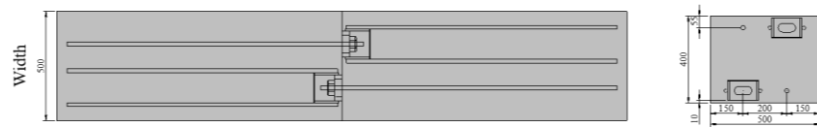
²⁾ A connector consisted of a steel shoe, two anchor bars (16 mm-diameter), and a connection bar (20 mm-diameter)



(a) Front view of specimens and details of steel shoe connectors



(b) Top view and section of S1 and S2: 1 Pair of connectors



(c) Top view and section of S3: 2 Pairs of connectors (Antisymmetric)



(d) Top view and section of S4: 2 Pairs of connectors (Bisymmetric)



(e) Top view and section of S5: 3 Pairs of connectors

Fig. 2 Configuration and dimensions of test specimens (units: mm)

All specimens measured $d = 400$ mm in depth (Fig. 2). The total length of test specimens was 2600 mm, and the clear length between supports was $L = 2400$ mm. For connectors, a product of Peikko Group Corporation (2016) was used. Each connector embedded in a PC wall segment consisted of a steel shoe (or steel box of outside width \times height \times depth = $140 \times 128 \times 93$ mm, having a hole in the bottom to enable a connection bar to pass through) and two anchor bars (16 mm-diameter deformed bars welded to the steel shoe) bolted to a connection bar (20 mm-diameter deformed bar) embedded in the adjacent PC wall segment. The hole for each connector was slotted to accommodate construction tolerances.

Because the connection bar and two anchor bars have different section and surface, arrangement of multiple connectors can affect structural performance of PC wall – steel shoe composite assemblies. The width of each test specimen also needs to be examined considering the arrangement of steel shoe connectors. Therefore, each specimen had different width and joint details. In the control specimen S1 having a width of $b = 300$ mm, a pair of connectors were placed at tension and compression sides, and structural adhesive resin (or epoxy resin: specified tensile strength = 48.3 MPa at 7 days) was applied at the mid-span joint for better bond. In S2 having the same width and connectors with S1, a rubber strip (3 mm) was provided at the midspan joint using a waterproof tape (high viscosity double side butyl rubber sealant tape), instead of applying the structural adhesive, because water-tightness is required for underground structures. In S3, the width was increased to $b = 500$ mm, and two pairs of connectors, antisymmetric in the direction, were placed. In S4, two pairs of connectors were bisymmetrically arranged, and the width was increased to $b = 600$ mm. In S5, three pairs of connectors were placed within a width of $b = 700$ mm. At the mid-span joints of S3, S4, and S5, the structural adhesive resin was also applied.

The D16 anchor bars and D20 connection bars (HRB500 steel in Chinese standards) functioned as flexural reinforcement. For transverse reinforcement, D8 deformed bars (HRB300 steel in Chinese standards) were placed at a spacing of 200 mm (the first transverse bar was located at 130 mm from the joint face). Considering connector size and environmental conditions for underground structures, minimum thickness of concrete cover for reinforcement was set as 45 mm.

2.2 Material properties

For test specimens, ready-mixed concrete of C50 was used. Since the concrete was delivered in twice, 100 mm cubes were taken for each delivery. For the cubes, compressive strength tests were carried out according to ASTM C109 (2011). Two concrete mixtures showed nearly identical properties. The average 28-day cube strength was $f'_{c,cube} = 42.6$ (left segment of each specimen) or 43.1 MPa (right segment of each specimen). The cube strength was converted into the cylinder strength f'_c by the strength class conformity of Eurocode 2 (2004) in order to take into account the size effect. The modulus of elasticity

Table 2 Compressive strength of concrete

Mixture ¹⁾	Measured 28-day Cube Strength	Converted Cylinder Strength ²⁾	Estimated Modulus of Elasticity ³⁾	Estimated Modulus of Rupture ³⁾
C50-1	42.6 MPa	33.5 MPa	27.2 GPa	3.6 MPa
C50-2	43.1 MPa	33.8 MPa	27.3 GPa	3.6 MPa

¹⁾ Ready-mixed concrete was delivered in twice;

²⁾ Converted based on the strength class conformity of Eurocode 2 (2004);

³⁾ Estimated based on the equations of ACI 318 (2014): $E_c = 4700\sqrt{f'_c}$, $f_r = 0.62\sqrt{f'_c}$

Table 3 Measured mechanical properties of reinforcement

Nominal diameter	Nominal area	Elastic modulus	Yield strength	Ultimate strength
16 mm (Anchor Bars)	201.1 mm ²	202 GPa	512 MPa	649 MPa
20 mm (Connection Bars)	314.2 mm ²	204 GPa	527 MPa	645 MPa
8 mm (Transverse Bars)	50.3 mm ²	210 GPa	270 MPa	420 MPa

$E_c = 4700\sqrt{f'_c}$ and modulus of rupture $f_r = 0.62\sqrt{f'_c}$ of concrete were estimated based on the equations of ACI 318 (2014). Table 2 summarizes the results.

For reinforcement, direct tension tests were carried out according to ASTM E8 (2009). Table 3 summarizes the test results. The average elastic modulus (E_s), yield strength (f_y), and ultimate strength (f_u) were 202 GPa, 512 MPa, and 649 MPa for 16 mm-diameter anchor bars (HRB500). $E_s = 204$ GPa, $f_y = 527$ MPa, and $f_u = 645$ MPa for 20 mm-diameter connection bars (HRB500), and $E_s = 210$ GPa, $f_y = 270$ MPa, and $f_u = 420$ MPa for 8 mm-diameter transverse bars (HRB300).

2.3 Production and connection

Fig. 3 shows the production and connection of the test specimens. A pair of PC wall segments were produced under the same conditions. To ensure accurate location of connectors, steel moulds were used for the joint faces, and steel shoes and connection bars were fixed in location by bolting before concrete placement. To prevent permeation of concrete, the opening of steel shoes was covered with Styrofoam, and concrete was poured and vibrated carefully. The PC wall segments were steam-cured for 12 hours, and then stored under room conditions.

At 21 days after concrete placement, a pair of PC wall segments were connected to each other. Before connecting them, the joint faces were cleaned by brush and then covered with structural adhesive resin (S1, S3, S4, S5) or waterproof tape (S2). To ensure alignment and complete contact of the two PC wall segments, the connection bars were carefully adjusted within the tolerance of the slotted hole in steel shoes. The connection bars were bolted by



Fig. 3 Production and connection of test specimens

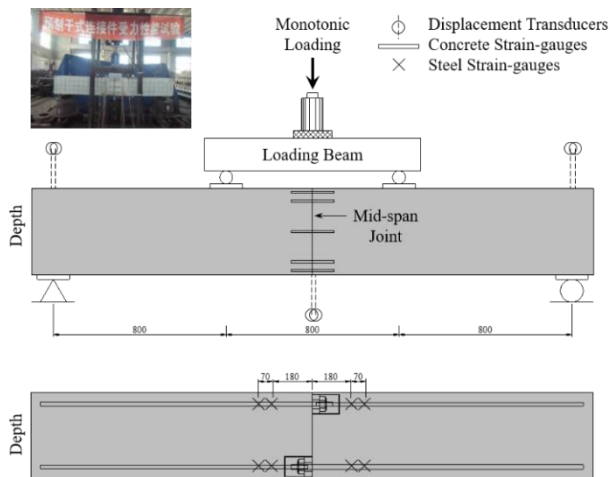


Fig. 4 Test Setup and Instrumentation (units: mm)

hand-wrenching (no further torque or grouting). The connected test specimens were kept untouched for another 7 days for bonding of the structural adhesive resin or waterproof tape.

2.4 Test setup and instrumentation

Fig. 4 shows the test setup and instrumentation. The test setup was prepared so that test specimens would be dominated by flexural behavior. Each specimen was simply-supported and tested under four-point loading conditions (distance between two loading points = $L/3$), in which the mid-span joint between two PC wall segments was subjected to the maximum bending moment. Vertical loading was applied through a 1 MN hydraulic jack, and a loading beam (I-shaped steel beam) was used for four-point loading. To prevent local failure, steel shim plates were placed at the loading points. Testing was carried out at the age of 28 days according to GB/T 50081 (2003), and loading was intermittently stopped and resumed to check

cracking and joint spacing.

For each specimen, six displacement transducers were installed to measure vertical displacements (2 at mid-span, and 4 at supports to check any movement of supports and to obtain the net displacement at mid-span). To measure concrete strains, five concrete strain-gauges (gauge-length = 100 mm) were attached on the concrete surfaces at the mid-span (with the distances of 20, 60, 200, 340, and 380 mm from the extreme compression fiber). To measure strains of anchor bars and connection bars, steel strain-gauges (two for each bar with the distances of 180 and 250 mm from the joint face) were also attached on the steel surfaces. The development and propagation of cracks were marked on the concrete surface, and crack width was measured using vernier calipers.

3. Test results

3.1 Failure mode

Fig. 5 shows the test specimens after testing and crack distribution. To identify the development and propagation of cracks, each crack was plotted commencing with the load at which the crack began to form. The test specimens showed flexural damage patterns combined with the rotational deformation of the two PC segments due to joint opening.

In the case of S1, S3, S4, and S5 (Figs. 5(a), (c), (d), and (e)), where the structural adhesive resin was applied at the mid-span joint, the first crack appeared at the mid-span joint, which is the critical section in terms of structural integrity and bending moment distribution. The joint crack rapidly propagated upwards (split open in a brittle manner), and the concrete surrounding connectors at the tension side was pulled apart. Under further loading, the opening of the mid-span joint gradually increased, and the rotation of two PC wall segments was observed. Narrow flexural cracks appeared at the lower part of two PC wall segments, and the

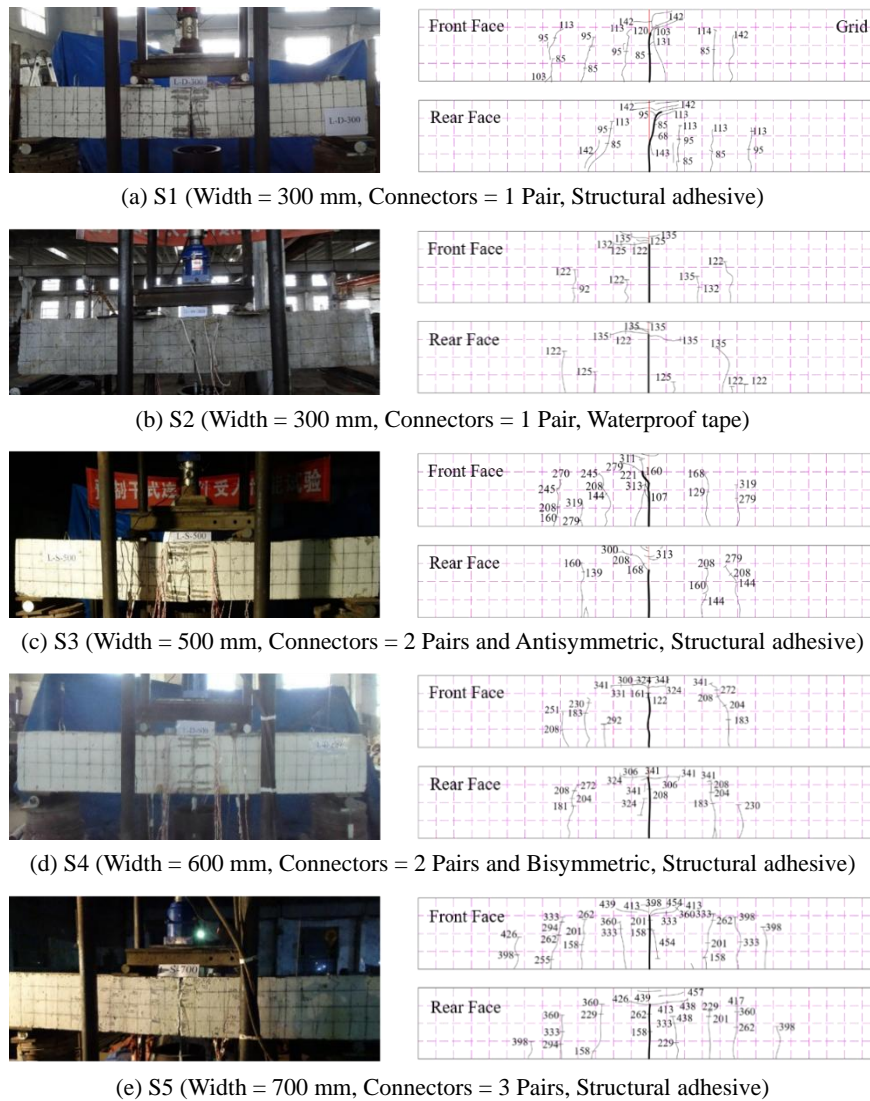


Fig. 5 Test specimens after testing and crack distribution (units: kN)

flexural cracks grew wider and propagated to the upper part. However, the flexural cracks were not as severe as those in general monolithic RC beams because of the joint opening at mid-span. Finally, concrete crushing occurred along the compression side around mid-span just before application of the peak load, and vertical displacement and rotation increased drastically, upon reaching the ultimate state. There were no distinct differences in the failure mode among S1, S3, S4, and S5, and also there were no significant differences in the flexural cracks between the two PC wall segments, indicating that arrangement of steel shoe connectors had no significant effect on failure mode.

In the case of S2 (Fig. 5(b)), where the waterproof tape was applied, the mid-span joint split open and the rotation of two PC wall segments was observed from the onset of initial loading. Under further loading, vertical displacement and rotation were retarded (two PC wall segments started directly contact each other at the compression side) and flexural cracks appeared. Finally, concrete crushing occurred, and the test specimen reached its ultimate state. The different failure mode of S2 from the other specimens was attributed to the rubber strip, which created an initial

gap of 3 mm between two PC wall segments. Specifically, the following three causes appeared to be responsible for the different failure mode: (1) elastic compression of the rubber strip and its nonsignificant contribution to tension; (2) initial strains in flexural bars caused by initial rotation; and (3) the depth of neutral axis required to be in equilibrium whereby the contact zone of concrete between two PC wall segments could provide resistance to compression even after the rubber strip was compressed.

Failure modes confirmed that the mid-span joint was structurally the weak plane, more pronounced in the case of applying waterproof tape instead of structural adhesive. After occurrence of joint cracking, joint opening could be excessive. Since joint opening could affect serviceability (such as water-leakage), concern should be given to it in design.

3.2 Load – displacement relationship

Fig. 6 shows the load – displacement relationship. Load V indicates the total vertical load measured from the load cell, and displacement δ indicates the net vertical

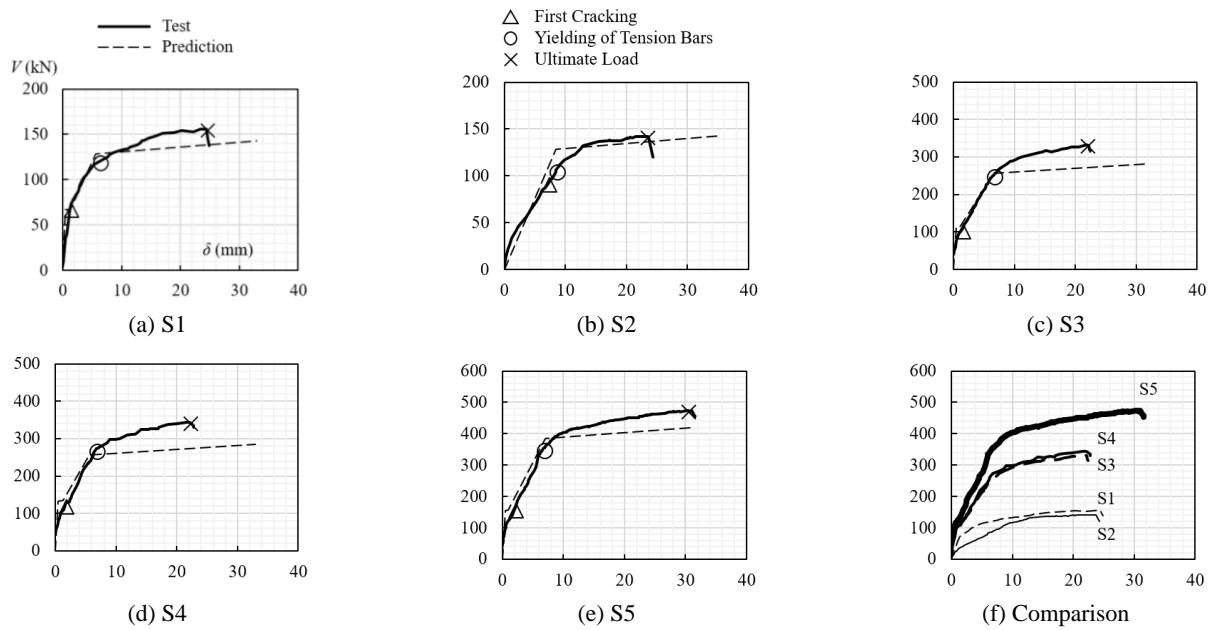


Fig. 6 Load – displacement relationship

Table 4 Test results

Specimen	First cracking ¹⁾			Yielding of tension bars			Ultimate load		
	V_{cr} (kN)	δ_{cr} (mm)	$V_{cr,exp}$ ²⁾ (kN)	V_y (kN)	δ_y (mm)	k_e ³⁾ (kN/m)	V_u (kN)	δ_u (mm)	μ ⁴⁾
S1	67.6	1.2	66.7	119.8	6.2	19230	156.0	24.4	3.9
S2	91.7	7.2	-	105.4	8.5	12468	142.2	23.3	2.8
S3	105.3	1.4	111.2	250.4	6.5	38356	332.7	21.8	3.3
S4	122.2	1.6	133.5	270.2	6.7	40483	343.9	22.1	3.3
S5	158.3	2.0	155.7	350.1	6.6	52702	473.9	30.3	4.6

1) First cracking indicates joint cracking at mid-span, except for S2 (flexural cracking along the PC wall segments)

2) Expected load at the mid-span cracking was calculated from Eq. (1c) (not valid for S2 because of the initial gap)

3) Effective flexural stiffness $k_e = V_y/\delta_y$

4) Displacement ductility $\mu = \delta_u/\delta_y$

displacement at mid-span, which was obtained by deducting the measured average displacement at supports from the measured average displacement at mid-span. In Fig. 6(a) through Fig. 6(e), solid lines depict test results, dashed lines are theoretical predictions, which will be discussed in the next section, and triangles, circles, and crosses indicate the first cracking, yielding of tension bars, and ultimate load, respectively. The test results are compared in Fig. 6(f) and summarized in Table 4. For better understanding, the concrete strain distribution along the depth of each specimen at various load levels and the load – steel strain relationship at the mid-span are given in Figs. 7 and 8. It is noted that the concrete strains shown in Fig. 7 were values affected by rotation, and S2 and some data of S5 were missed in Fig. 7 due to the damage of concrete strain-gauges. Each steel strain in Fig. 8, assuming linear strain distribution along the length of the bar, was obtained from two measured strains along the bar, because the installation of steel strain-gauges at the midspan was not possible due to the joint.

During loading, the flexural responses of the test specimens were categorized into three phases based on the behavior of the mid-span joint and connectors: (1) elastic response before joint cracking (uncracked response); (2) response before yielding of tension bars (pre-yield response); and (3) response after yielding of tension bars (post-yield response) until concrete crushing.

In the control specimen S1 (width = 300 mm, connectors = 1 pair, and structural adhesive: see Fig. 6(a)), the load linearly increased before the first cracking at the mid-span joint, and the first crack (joint crack) appeared at $V_{cr} = 67.6$ kN. The displacement at cracking was $\delta_{cr} = 1.2$ mm. Because the structural adhesive had the higher tensile strength than concrete, the cracking load V_{cr} was quite similar to the expected cracking load $V_{cr,exp} = 66.7$ kN ($V_{cr} = 101\%$ of $V_{cr,exp}$), which can be calculated based on the elastic beam theory (Wight and MacGregor 2011) and the equation of ACI 318 (2014) for cracking moment M_{cr} (Eq. (1)).

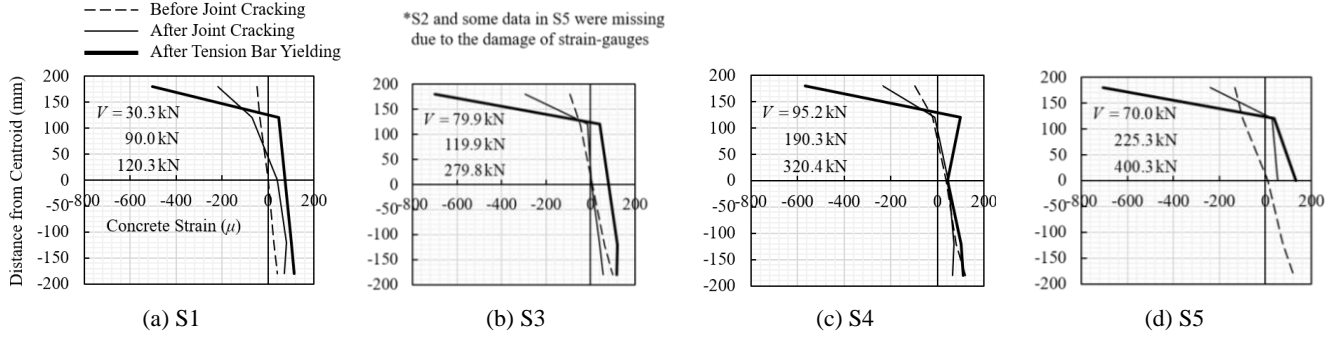


Fig. 7 Concrete strain distribution

$$M_m = \frac{wL^2}{8} + \frac{VL}{6} \quad (1a)$$

$$M_{cr} = \frac{f_r I_g}{y_t} \quad (1b)$$

$$V_{cr,exp} = \left(\frac{f_r I_g}{y_t} - \frac{wL^2}{8} \right) \frac{6}{L} \quad (1c)$$

where M_m = maximum moment occurring for the conditions under consideration; $wL^2/8$ = moment at mid-span due to self-weight of $w = bd\rho$; $\rho = 24 \text{ kN/m}^3$ = density of RC (Wight and MacGregor 2011); $VL/6$ = moment at mid-span due to external load (or four-point loading); $I_g = bd^3/12$ = moment of inertia of gross section about centroidal axis, neglecting reinforcement; and $y_t = d/2$ = distance from centroid of section to extreme tension fiber.

After the first cracking, the slope of the load – displacement curve gradually decreased, and the concrete strain at the compression side sharply increased (Fig. 7(a)). At $V_y = 119.8 \text{ kN}$, the D20 connection bar in tension yielded prior to the two D16 anchor bars (Fig. 8(a)), and the slope of the load – displacement curve was decreased more rapidly. The displacement at yielding was $\delta_y = 6.2 \text{ mm}$, and the effective flexural stiffness was estimated as $k_e = V_y/\delta_y = 19230 \text{ kN/m}$. At $\delta_u = 24.4 \text{ mm}$, the load reached its maximum ($V_u = 156.0 \text{ kN}$) and suddenly dropped. The displacement ductility was estimated as $\mu = \delta_u/\delta_y = 3.9$.

In S2 (width = 300 mm, connectors = 1 pair, and waterproof tape: see Figs. 6(b) and 8(b)), the mid-span joint split open from the initial loading because of the initial gap (or rubber strip), and concrete strain-gauges were damaged (thus, no data for S2 in Fig. 7). Flexural cracks (not a joint crack) developed along the PC wall segments at $V_{cr} = 91.7 \text{ kN}$ ($\delta_{cr} = 7.2 \text{ mm}$). The yielding of the D20 connection bar in tension occurred at $V_y = 105.4 \text{ kN}$, and the ultimate load was $V_u = 142.2 \text{ kN}$. The load-carrying capacity (V_y and V_u) was similar to that of S1, but the yield displacement ($\delta_y = 8.5 \text{ mm}$) was greater than that of S1 resulting in reduction of the effective flexural stiffness ($k_e = V_y/\delta_y = 12468 \text{ kN/m}$) and displacement ductility ($\mu = \delta_u/\delta_y = 2.8$, where $\delta_u = 23.3 \text{ mm}$). As mentioned previously, the greater yield displacement was caused by the initial gap.

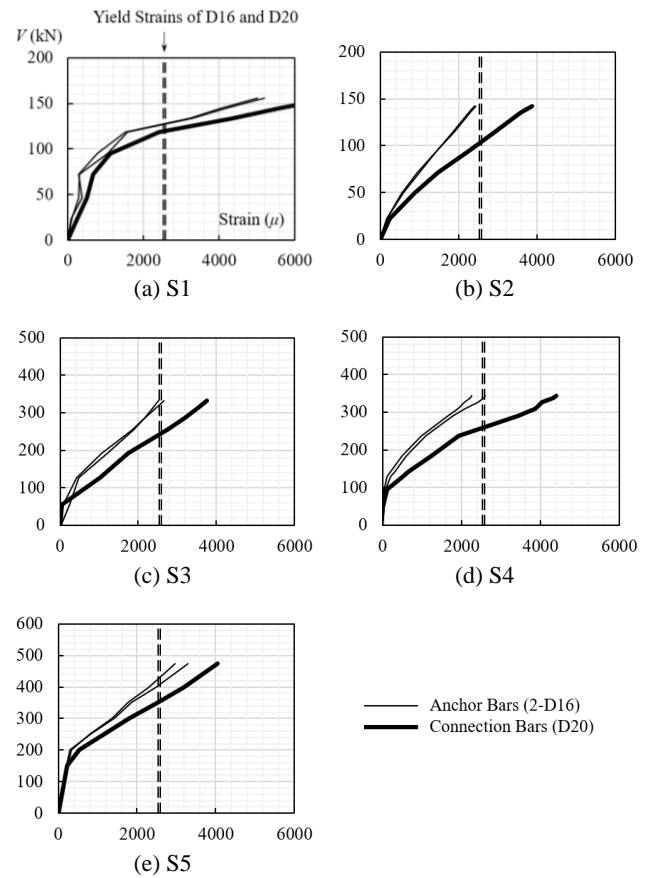


Fig. 8 Load – steel strain relationship at mid-span

In S3 (width = 500 mm, connectors = 2 pairs and antisymmetric, and structural adhesive: see Figs. 6(c), 7(b), and 8(c)), joint cracking began at $V_{cr} = 105.3 \text{ kN}$ (95% of $V_{cr,exp}$, $\delta_{cr} = 1.4 \text{ mm}$), steel yielding occurred at $V_y = 250.4 \text{ kN}$ ($\delta_y = 6.5 \text{ mm}$, $k_e = V_y/\delta_y = 38356 \text{ kN/m}$), and ultimate load was $V_u = 332.7 \text{ kN}$ ($\delta_u = 21.8 \text{ mm}$, $\mu = \delta_u/\delta_y = 3.3$). In S4 (width = 600 mm, connectors = 2 pairs and bisymmetric, and structural adhesive: see Figs. 6(d), 7(c), and 8(d)), joint cracking began at $V_{cr} = 122.2 \text{ kN}$ (92% of $V_{cr,exp}$, $\delta_{cr} = 1.6 \text{ mm}$), steel yielding occurred at $V_y = 270.2 \text{ kN}$ ($\delta_y = 6.7 \text{ mm}$, $k_e = V_y/\delta_y = 40483 \text{ kN/m}$), and ultimate load was $V_u = 343.9 \text{ kN}$ ($\delta_u = 22.1 \text{ mm}$, $\mu = \delta_u/\delta_y = 3.3$). Although S3 and S4 were different in width and connector arrangement, their overall behaviors

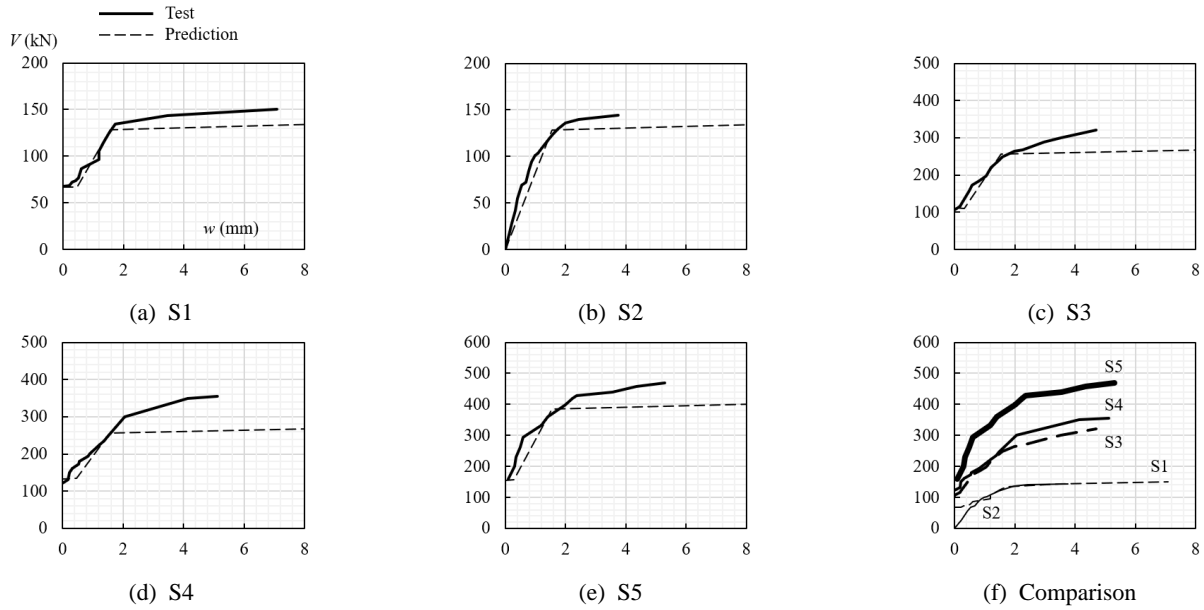


Fig. 9 Load – joint opening relationship

were quite similar. This is attributed to the capacity of the connector, which was controlled by a D20 connection bar (having the smaller section and surface) rather than two D16 anchor bars. In short, effective flexural bars were same in both S3 and S4, regardless of the connector arrangement. This indicates that the arrangement of connectors has no significant effect on the structural performance and the antisymmetric arrangement (in S3) would be better because the bisymmetric or parallel arrangement (in S4) needs wider width to ensure proper clearance of surrounding concrete for each connector. The slightly greater load-carrying capacity of S4 was attributed to the wider width on the compression side.

In S5 (width = 700 mm, connectors = 3 pairs, and structural adhesive: see Figs. 6(e), 7(d), and 8(e)), joint cracking began at $V_{cr} = 158.3$ kN (102% of $V_{cr,exp}$, $\delta_{cr} = 2.0$ mm), steel yielding occurred at $V_y = 350.1$ kN ($\delta_y = 6.6$ mm, $k_e = V_y/\delta_y = 52702$ kN/m), and ultimate load was $V_u = 473.9$ kN ($\delta_u = 30.3$ mm, $\mu = \delta_u/\delta_y = 4.6$). Due to the larger number of connectors, the wider width, and the lesser pulling-apart of the concrete surrounding connectors at the tension side, S5 showed the better performance (higher strength and ductility).

In conclusion, the PC wall – steel shoe composite assemblies showed satisfactory structural performance, regardless of the arrangement of steel shoe connectors. However, in the case of applying waterproof tape (instead of structural adhesive), the effective flexural stiffness and ductility were decreased due to the initial gap.

3.3 Joint opening

Fig. 9 shows the load – joint opening relationship. In the figure, solid lines are the test results, and dashed lines are predictions which will be discussed in the next section. As shown in the figure, the joint began to open after the joint cracking (or from the initial loading in S2), and the joint opening was increased as the load increased. However, the

joint opening was not excessive at service load levels (around 2 mm in all specimens). This indicates the serviceability of the PC wall – steel shoe composite assemblies was acceptable. In the case of introducing a proper level of initial compression (such as higher torque in bolting, prestressing tendons, or gravity loads), joint opening could be reduced.

4. Discussions

4.1 Flexural strength

For strength design of PC wall – steel shoe composite assemblies, a theoretical model for flexural strength was proposed. The test results showed that the total deformation of PC wall – steel shoe composite assemblies can be decomposed into two deformation components: (1) flexural deformation by bending; and (2) rotational deformation due to joint opening. Since thickness of PC wall – steel shoe composite assemblies is small in comparison to their height/length, resulting in a large shear span-to-depth ratio, shear deformation was not considered.

Flexural deformation by bending was calculated based on the elastic beam theory (Wight and MacGregor 2011) and the concept of the effective moment of inertia specified in ACI 318 (2014). Considering the self-weight w and external load V (Fig. 10(a)), the vertical displacement δ_b at the mid-span by bending can be calculated as follows

$$\delta_b = \frac{5wL^4}{384E_cI_e} + \frac{23VL^3}{1296E_cI_e} \quad (2a)$$

$$I_e = \left(\frac{M_{cr}}{M_m}\right)^3 I_e + \left[1 - \left(\frac{M_{cr}}{M_m}\right)^3\right] I_{cr} \leq I_g \quad (2b)$$

$$I_{cr} = nA_s(d_s - c)^2 + \frac{bc^3}{3} \quad (2c)$$

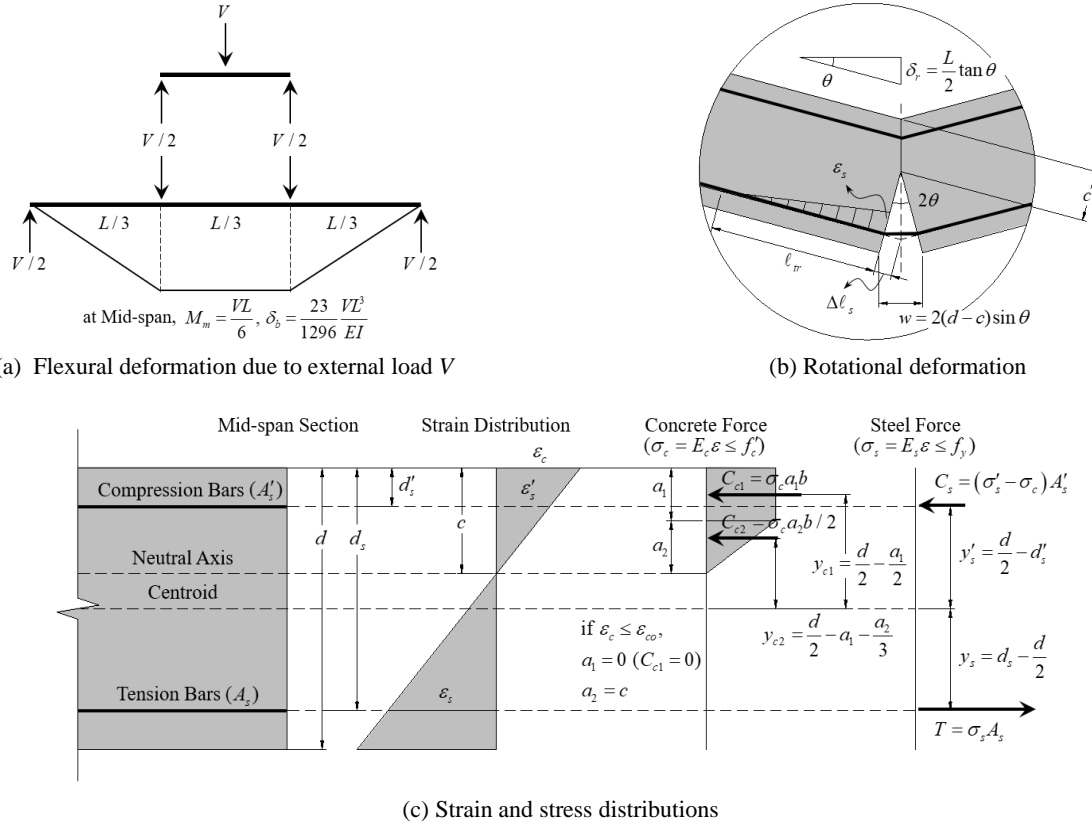


Fig. 10 Deformation of PC wall – steel shoe composite assemblies

where $5wL^4/384E_cI_e$ = displacement at mid-span due to self-weight; $23VL^3/1296E_cI_e$ = displacement at mid-span due to external load (or four-point loading); I_e = effective moment of inertia for calculation of deflection; I_{cr} = moment of inertia of cracked section transformed to concrete (without axial force); $n = E_s/E_c$ = modular ratio; A_s = area of tension bars; b, d = width and depth of section; d_s = distance from extreme compression fiber to centroid of tension bars; and c = distance from extreme compression fiber to neutral axis. In the calculation of the neutral axis depth c , the effect of the rotational deformation should be considered.

Rotational deformation due to joint opening (when $M_m > M_{cr}$) is associated with the elongation of tension bars. To calculate elongation of tension bars, strain of the tension bars was assumed to vary linearly along the transfer length (Fig. 10(b)). Thus, elongation Δl_s of tension bars can be calculated as follows

$$\Delta l_s = \int_0^{\ell_{tr}} \varepsilon_s dz = \frac{1}{2} \varepsilon_s \ell_{tr} \quad (3)$$

where ε_s = strain of tension bars; $\ell_{tr} = (\sigma_{se}/21)d_b$ = transfer length (ACI 318 2014); σ_{se} = effective stress in tension bars (in this study, σ_{se} was assumed to be identical with the steel stress σ_s); and d_b = nominal diameter of a tension bar (not anchor bars, but connection bar).

Based on plane section assumption, strain-compatibility, and geometry conditions, the elongation Δl_s of tension bars can be defined as a function of rotation angle θ (Eq.

(4)), and the strain ε_s of tension bars and strain ε_c of compression concrete can be defined as Eq. (5) from Eqs. (3) and (4).

$$\Delta l_s = (d_s - c)\tan\theta \quad (4)$$

$$\varepsilon_s = \frac{2(d_s - c)\tan\theta}{\ell_{tr}} \quad (5a)$$

$$\varepsilon_c = \frac{c}{d_s - c} \varepsilon_s = \frac{2c\tan\theta}{\ell_{tr}} \quad (5b)$$

For design purpose, the bilinear stress-strain relationship of Eurocode 2 (2004) was used for concrete (Eq. (6)), and steel bars were assumed to be elasto-plastic (Eq. (7)).

$$\sigma_c = \frac{f'_c}{\varepsilon_{c0}} \varepsilon \leq f'_c \quad (\sigma_c = 0 \text{ if } \varepsilon > \varepsilon_{cu}) \quad (6)$$

$$\sigma_s = E_s \varepsilon \leq f_y \quad (7)$$

where σ_c = stress of concrete corresponding to strain ε ; σ_s = stress of steel corresponding to strain ε ; and $\varepsilon_{c0}, \varepsilon_{cu}$ = concrete strain at peak stress and ultimate strain (assumed as 0.00175 and 0.0035 (Eurocode 2 2004)).

For a given rotation θ , the neutral axis depth c satisfying the force equilibrium of Eq. (8a) can be determined by iterations, and the internal bending moment and shear force can be calculated as Eqs. (8b) and (8c).

$$P = C_{c1} + C_{c2} + C_s - T = 0 \quad (8a)$$

$$M = C_{c1}y_{c1} + C_{c2}y_{c2} + C_s y_s' - T y_s \quad (8b)$$

$$V = \left(M - \frac{wL^2}{8} \right) \frac{6}{L} \quad (8c)$$

where P = internal axial force; M = internal bending moment; V = internal shear force; C_{c1}, C_{c2} = compression forces of concrete corresponding to rectangular and triangle stress distributions; C_s, T = forces of compression and tension bars; and $y_{c1}, y_{c2}, y_s', y_s$ = moment-arms or distances from centroid of section to resultant forces (C_{c1}, C_{c2}, C_s, T). The calculations of the resultant forces and moment-arms are given in Fig. 10(c) in the same way for the design of doubly reinforced beams.

The vertical displacement δ_r by rotation at the mid-span can be calculated as Eq. (9), and the total displacement δ is the sum of the two deformation components (Eq. (10)).

$$\delta_r = \frac{L}{2} \tan\theta \quad (9)$$

$$\delta = \delta_b + \delta_r \quad (10)$$

Flexural responses of the test specimens can be composed of four points (except the origin) based on the test results: the 1st point at cracking load (V from Eq. (1c) and δ from Eq. (2a) using I_g); the 2nd point just after cracking (V from Eq. (8c) and δ from Eq. (10) using I_e from Eq. (2b)) when $V = V_{cr,exp}$; the 3rd point at steel yielding (same with the 2nd point but when $\varepsilon_s = \varepsilon_y = f_y/E_s$); and the 4th point at concrete crushing (same with the 2nd point but when $\varepsilon_c = \varepsilon_{cu}$). In the case of S2, due to the initial gap, the first and second points did not exist and $M_{cr} = 0$ in the calculation of I_e from Eq. (2b).

In Fig. 6(a) through Fig. 6(e), predictions (dashed lines) were compared with the test results (thick solid lines) to verify the proposed model. Although the proposed model underestimated the ultimate load due to ignorance of the strain-hardening effect of flexural bars and the confinement effect of transverse bars, the proposed model was deemed acceptable for design purpose considering its simplicity and exactness.

4.2 Joint opening

Since the opening of the mid-span joint affects the serviceability of underground structures, joint openings need to be considered in the design of PC wall – steel shoe composite assemblies. Based on the proposed model, the joint opening w can be estimated as follows (Fig. 10(b))

$$w = 2(d - c)\sin\theta \quad (11)$$

As shown in Fig. 9(a) through Fig. 9(e), the proposed model (dashed lines) approximated joint opening well at service load levels, indicating that the joint opening can be predicted with design parameters in the design step using the proposed model.

5. Conclusions

To investigate the flexural behavior of PC wall – steel shoe composite assemblies with various dry connection details, flexural tests were performed for five scenarios. Test parameters included the width of test specimens, arrangement of steel shoe connectors, and use of structural adhesive or waterproof tape at the mid-span joint. Based on the test results, the flexural strength and joint spacing, which are required for strength and serviceability design, were discussed theoretically. The conclusions from the experimental and theoretical investigations are summarized as follows:

- The PC wall – steel shoe composite assemblies joined at mid-span by dry connection showed flexural damage patterns combined with the rotational deformation of the two PC segments due to joint opening. Based on the behavior at the mid-span joint and connectors, the flexural response can be categorized into three phases: (1) elastic response before joint cracking (uncracked response); (2) response before yielding of tension bars (pre-yield response); and (3) response after yielding of tension bars (post-yield response) until concrete crushing.
- The PC wall – steel shoe composite assemblies showed satisfactory structural performance, regardless of the arrangement of steel shoe connectors. However, in the case of applying waterproof tape (instead of structural adhesive), the effective flexural stiffness and ductility were decreased due to the initial gap. Since joint openings could affect the serviceability of underground structures (such as water-leakage), concern should be given to joint opening connections in design.
- Considering two deformation components (flexural deformation by bending and rotational deformation due to joint opening), a theoretical model for flexural strength and joint opening was proposed based on plane section assumption, strain-compatibility, and geometry conditions.
- The proposed model was deemed acceptable for design purpose considering its simplicity and exactness. Using the proposed model, flexural strength can be estimated, and joint opening can be predicted with design parameters in the design step.

Further research on PC wall – steel shoe composite assemblies using dry connection should be continued, particularly regarding the behavior subjected to combined bending and axial force or combined bending and shear, which can affect both load-carrying capacity and serviceability.

Acknowledgments

This research was supported by the following sponsors or grants: National Natural Science Foundation of China (Grant No. 51878222 and 51678196); the NSFC-NRF joint project (51811540401); Research and Development Project

of the Ministry of Housing and Urban-Rural Development of P.R.C (K92017039); Heilongjiang Province Natural Science Fund (E2015014); and NRF-NSFC Joint Collaborative Fund (Korea Grant No. 2018K2A9A2A06011014 and China Grant No. 5171102182). The authors are grateful to the authorities for their supports.

References

- ACI Committee 318 (2014), Building Code Requirements for Structural Concrete and Commentary (ACI 318), American Concrete Institute; Farmington Hills, MI, USA.
- American Society for Testing and Materials (2009), Standard Test Methods for Tension Testing of Metallic Materials (ASTM E8), American Society for Testing and Materials; West Conshohocken, PA, USA.
- American Society for Testing and Materials (2011), Standard Test Method for Compressive Strength of Hydraulic Cement Mortars (Using 2-in. or [50-mm] Cube Specimens) (ASTM C109); American Society for Testing and Materials; West Conshohocken, PA, USA.
- Aparicio, A.C., Ramos, G. and Casas, J.R. (2002), “Testing of externally prestressed concrete beams”, *Eng. Struct.*, **24**, 73-84.
- Centre for Advanced Engineering (CAE) (1999), Guidelines for the Use of Structural Precast Concrete in Buildings; Wickliffe Press, New Zealand.
- Cheng, C.T. (2008), “Seismic behavior of post-tensioned precast reinforced concrete beam-to-column connections”, *Comput. Concrete, Int. J.*, **5**(6), 525-544.
- Elliott, K.S. (2002), *Precast Concrete Structures*, Butterworth-Heinemann, Woburn, MA, USA.
- Englekirk, R.E. (2003), *Seismic Design of Reinforced and Precast Concrete Buildings*, John Wiley & Sons, Inc., Hoboken, NJ, USA.
- European Committee for Standardization (2004), Design of Concrete Structures – Part 1-1: General Rules and Rules for Buildings (Eurocode 2); Brussels, Belgium.
- Han, C., Li, Q., Wang, X., Jiang, W. and Li, W. (2016), “Research on rotation capacity of the new precast concrete assemble beam-column joints”, *Steel Compos. Struct., Int. J.*, **22**(3), 613-625.
- International Federation for Structural Concrete (fib) (2008), *fib Bulletin 43: Structural Connections for Precast Concrete Buildings*, Sprint-Digital-Druck, Stuttgart, Germany.
- Jiang, H., Cao, Q., Liu, A., Wang, T. and Qiu, Y. (2016a), “Flexural behavior of precast concrete segmental beams with hybrid tendons and dry joints”, *Constr. Build. Mater.*, **110**, 1-7.
- Jiang, H., Chen, Y., Liu, A., Wang, T. and Fang, Z. (2016b), “Effect of high-strength concrete on shear behavior of dry joints in precast concrete segmental bridges”, *Steel Compos. Struct., Int. J.*, **22**(5), 1019-1038.
- Joint Research Centre (JRC) (2012), Design Guidelines for Connections of Precast Structures under Seismic Actions; European Union, Luxembourg.
- Kang, T.H.-K., Kim, W., Kwak, Y.-K. and Hong, S.-G. (2014), “Flexural testing of reinforced concrete beams with recycled concrete aggregates”, *ACI Struct. J.*, **111**(3), 607-616.
- Lee, J.D., Yoon, J.K. and Kang, T.H.-K. (2016), “Combined half precast concrete slab and post-tensioned slab topping system for basement parking structures”, *J. Struct. Integrity Maint.*, **1**(1), 1-9.
- Lim, Y.W. and Hong, S.G. (2014), “Cyclic loading tests for precast concrete cantilever walls with C-type connections”, *Earthq. Struct., Int. J.*, **7**(5), 753-777.
- National Standard of People’s Republic of China (2003), Standard for Test Method of Mechanical Properties on Ordinary Concrete (GB/T 50081); China Construction Industry Press; Beijing, China. [In Chinese]
- Ousaleem, H., Ishikawa, Y., Kimura, H., Kusaka, T., Yanagisawa, N. and Okamoto, K. (2009), “Seismic performance and flexural stiffness variation of assembled precast high-strength concrete beam jointed at mid-span using transverse bolts”, *J. Adv. Concrete Technol.*, **7**(2), 205-216.
- PCI Industry Handbook Committee (PCI) (2004), *PCI Design Handbook*, (6th Edition), Precast/Prestressed Concrete Institute, Chicago, IL, USA.
- Peikko Group Corporation (2016), Concrete Connections: Product Catalogue, Peikko Group, Finland.
- Saibabu, S., Srinivas, V., Sasmal, S., Lakshmanan, N. and Iyer, N.R. (2013), “Performance evaluation of dry and epoxy jointed segmental prestressed box girders under monotonic and cyclic loading”, *Constr. Build. Mater.*, **38**, 931-940.
- Vaghei, R., Hejazi, F., Taheri, H., Jaafar, M.S. and Ali, A.A.A. (2016), “A new precast wall connection subjected to monotonic loading”, *Comput. Concrete, Int. J.*, **17**(1), 1-27.
- Wight, J.K. and MacGregor, J.G. (2011), *Reinforced Concrete: Mechanics & Design*, (6th Edition), Pearson Education, Inc., Upper Saddle River, NJ, USA.

CC